Water Science & Technology

IWA PUBLISHING

Water Science & Technology Vol 87 No 7, 1660 doi: 10.2166/wst.2023.086

Effects of graphitic carbon nitride in the formation of disinfection byproducts

Linjie Ni[a,b], Jiaqi Hu[a,b], Jie Mao[a,b], Shanshan Li[a,b], Haitao Wang[a,b] and Jinfeng Lu[a,b,c,*]

[a] College of Environmental Science and Engineering, Nankai University, Tianjin 300071, China
[b] Tianjin Key Laboratory of Environmental Technology for Complex Trans-Media Pollution, Tianjin 300071, China
[c] Key Laboratory of Pollution Processes and Environmental Criteria (Nankai University), Ministry of Education, Tianjin 300071, China
*Corresponding author. E-mail: lujinfeng@nankai.edu.cn

ABSTRACT

Graphitic carbon nitride (CN) was a promising candidate for efficient environmental remediation in the advanced oxidation processes (AOPs). However, whether CN itself had some potential environmental risks, such as affecting the production of disinfection byproducts (DBPs) was still unknown. This study investigated the formation potential of DBPs in the presence of CN. The experimental data revealed that CN had a high potential to form DBPs, and dichloroacetonitrile (DCAN) was the most produced species during the chlorination and chloramination processes. Moreover, the effects of chlorine time, chlorine dosage, pH, and CN dosage during the chlorination process were evaluated to understand the formation pattern of DBPs. The possible mechanism of DBPs formation was deduced by analyzing the results of FTIR, Raman, and XPS before and after chlorination. Finally, the DBPs formation potential and cytotoxicity of the CN leaching solution were investigated, indicating CN could leach the precursors of DBPs and that the potential toxicity of the leaching solution increased with the extension of CN immersion time. In general, this research adds an understanding of the DBP formation of CN in water treatment systems and sheds light on CN's environmental potential risks.

Key words: chloramine, chlorine, dichloroacetonitrile, disinfection byproducts, graphitic carbon nitride, leaching

HIGHLIGHTS

- g-C_3N_4(CN) has a high potential to form DBPs and dichloroacetonitrile (DCAN) was the dominant species.
- Chorine dosage, pH, and CN dosage could significantly affect DBPs formation.
- Chlorine attacked the N-containing aromatic ring and the surface amino group of CN to produce DBPs.
- CN could leach the precursors of DBPs and DCAN was the major contributor to the formed DBPs cytotoxicity.

GRAPHICAL ABSTRACT

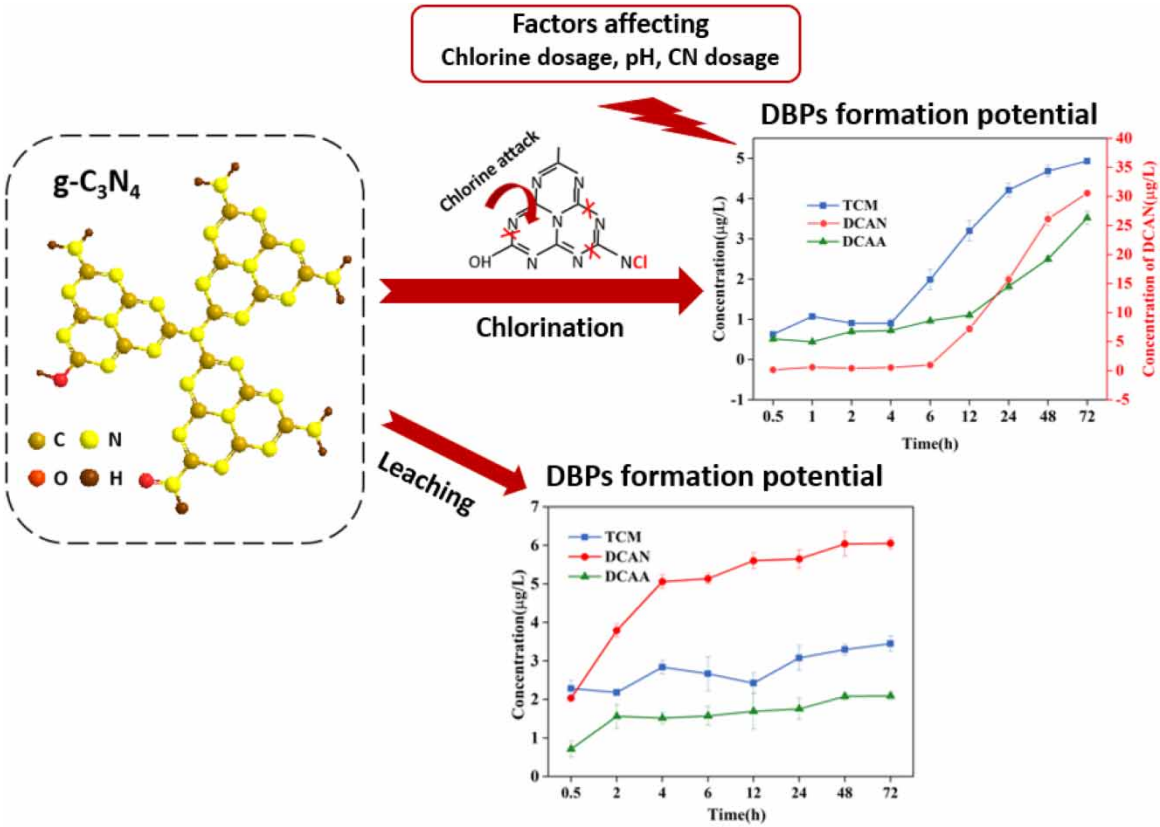

1. INTRODUCTION

Graphitic carbon nitride (g-C_3N_4), as a 2D metal-free conjugated polymer nanomaterial, has the advantages of simple synthesis, low cost, and excellent light absorption ability (Yang *et al.* 2020; John *et al.* 2021). In recent years, many researchers have confirmed that g-C_3N_4 is a promising candidate in the field of metal-free catalysts and photocatalytic activity (Zhu *et al.* 2018; Santosoa *et al.* 2020). For example, the g-C_3N_4-enabled advanced oxidation processes (AOPs) showed excellent ability to remove natural organic matter (NOM) and pharmaceutical personal care products (PPCPs) (Acharya & Parida 2020; Jiang *et al.* 2020). In particular, dosing g-C_3N_4 into the solar/chlorine AOP system has attracted much attention due to the effective adsorption of visible light and the high yield of active radicals (Stefán *et al.* 2019; Li *et al.* 2021a, 2021b). Nowadays, g-C_3N_4-based hybrid membranes also showed marvelous catalytic activities in the treatment of refractory organic compounds (Liu *et al.* 2017a, 2017b; Cheng *et al.* 2020; Ren *et al.* 2021). As shown in Figure 1, the number of publications per year on g-C_3N_4 increased rapidly from 397 to 3,628 in 2014–2021. With the increasing application of g-C_3N_4, the risk of g-C_3N_4 leaking into the environment has increased dramatically, and the physicochemical transformation of g-C_3N_4 by chlorine may occur in such membrane cleaning and chlorine AOP processes (Jazic *et al.* 2019).

Controlling the disinfection byproducts (DBPs) formation has always been a difficult task due to their teratogenic, carcinogenic, and mutagenic effects (Wongrueng *et al.* 2019). Many investigations have demonstrated that the reaction between NOM and chlorine could promote the formation of DBPs (Chen *et al.* 2017; Li *et al.* 2021a, 2021b). However, recent research indicated that residual carbon and nitrogen-containing materials were potential precursors of DBPs. Trihalomethanes (THMs) and halo acetic acids (HAAs) could be produced when graphene oxide (GO), activated carbon (AC), biochar, or carbon nanotubes (CNTs) reacted with chlorine or chloramine (Liu *et al.* 2018a, 2018b; Zhang *et al.* 2019; Huang *et al.* 2021). Since g-C_3N_4 has been unanimously recognized by researchers in water pollution treatment, it is likely to be applied on a large scale in the foreseeable future (Wang *et al.* 2017; Han *et al.* 2020). Whether g-C_3N_4 itself has some byproduct

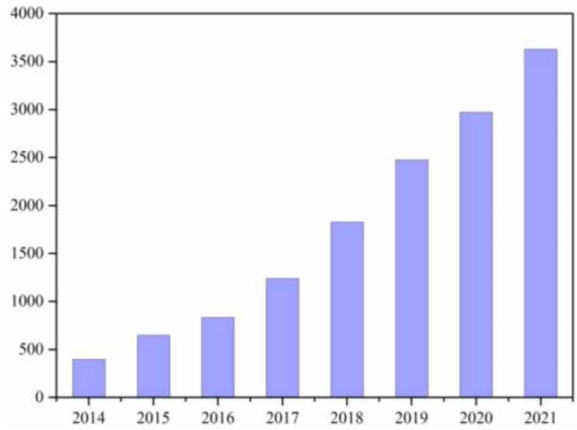

Figure 1 | The publications on g-C_3N_4 over time.

formation potential risks when exposed to chlorine is still unknown. It is imperative to assess the DBPs formation potential of g-C_3N_4.

Thus, the purpose of this work was to investigate the effects of g-C_3N_4 on the formation of DBPs. Trichloromethane (TCM), dichloroacetonitrile (DCAN), and dichloroacetic acid (DCAA) were detected to assess the DBPs formation potential of g-C_3N_4. Cl_2 dosage, solution pH, and g-C_3N_4 dosage were detected to evaluate the factors affecting DBPs formation. The properties of g-C_3N_4 before and after chlorination were determined to find out the possible mechanism of g-C_3N_4-formed DBPs. Furthermore, the formation of DBPs and corresponding theoretical cytotoxicity of the g-C_3N_4 leaching solution were investigated. These researches were significant both theoretically and practically in assessing the possible environmental risks of g-C_3N_4.

2. MATERIALS AND METHODS

2.1. Reagents and materials

The DBP standards utilized in this study were derived from Anpu Experimental Technology Co. Ltd (Shanghai, China). Anhydrous sodium sulfate (Na_2SO_4) was obtained from Sinopharm Chemical Reagent Co. Ltd (Tianjin, China). Methyl tert-butyl ether (MTBE) was purchased from Fisher Chemical (China). Sodium hypochlorite stock solution and urea were purchased from Maclin Biochemical Technology Co. Ltd (Shanghai, China). To remove residual chlorine, sodium sulfite (Tianjin Guangfu Fine Chemical Research Institute, China) was utilized.

The g-C_3N_4 was synthesized from urea. Typically, 15 g of urea was taken in alumina crucibles with a cover and calcined at 550 °C with a heating rate of 5 °C/min for 4 h and allowed to cool naturally to room temperature. The light yellow powders were collected by centrifugation and washed with ultrapure water several times. The sample was named CN.

2.2. Experiment procedures

Firstly, 250 mL ultrapure water mixed with 20 mg/L CN samples was added in a conical flask and the pH was adjusted to 7 with phosphoric acid buffer. The concentration of NaClO (as Cl_2) was identical at 1, 4, 10, and 20 mg/L. All samples were performed in the dark for 3 days at room temperature (25 $\pm$ 1 °C). After 72 h of chlorination, water samples were filtered by the 0.45 μm membrane. The chlorinated powders were collected and named as CN-Cl. The residual chlorine was quenched by sodium sulfite and the quenched sample was immediately extracted with MTBE. Finally, 1 mL upper layer of MtBE was taken out for gas chromatography (GC) detection. For comparison, the chloramination of CN was investigated. The monochloramine (NH_2Cl) solutions were freshly generated by adding NaClO solution gently into a stirred NH_4Cl solution with the Cl: N mass ratio of 4:1.

2.3. Analytical methods

TCM, DCAN, and DCAA were measured according to EPA 551.1 and 552.3 using GC (Agilent 6890N, Santa Clara, CA, USA) equipped with an electron capture detector (Agilent Technologies, Santa Clara, CA, USA). The column used for detection was

an HP-5 fused silica capillary column (30 mm × 0.25 mm I.D. with a film thickness of 0.25 mm). The pH of the water samples was measured through a pH meter (PHS-3G, Shanghai Yi Electrical Scientific Instrument Co. Ltd). Residual chlorine was investigated by using the N, N-diethyl-p-phenylenediamine (DPD) method. The dissolved organic carbon (DOC) and the total dissolved nitrogen (TDN) were measured by a TOC/TN analyzer (TOC-5000A; Shimadzu). The concentration of dissolved organic nitrogen (DON) was determined by subtracting inorganic nitrogen (NO_3^--N, NO_2^--N, NH_4^+-N) from TDN.

2.4. Characterization of CN

The morphologic changes of CN before and after chlorination were seen using a transmission electron microscope (HRTEM, JEM-1200EX). The surface area and pore size of CN were measured using a Brunauer–Emmett–Teller (BET) surface analyser (Quantachrome NOVA1000, USA). The functional groups were determined by using Fourier transform infrared spectroscopy analysis (FTIR, Bruker Tensor 27, Germany) and X-ray photoelectron spectroscopy (XPS, ESCALAB 250, Thermo Fisher Scientific). The variations in thickness were measured by atomic force microscopy (AFM, Bruker Dimension Icon, USA). The Raman spectra of samples were tested with a Raman spectrometer (SR-500I-A, 532 nm).

2.5. Analysis of the potential toxic risk of DBPs caused by CN

The toxicity values of various DBPs that provided evidence about cytotoxicity potentials have been investigated using the Chinese hamster ovary (CHO) cells (Jeong *et al.* 2015; Wagner & Plewa 2017). The CHO comprehensive cytotoxicity index (CTI) was determined by dividing the measured concentration of each DBP by the corresponding published median lethal concentration (LC_{50}) (Equation (1)). The evaluation of cytotoxicity could reliably understand the effective control of different species of DBPs due to the varied toxicity values. The LC_{50} value of each DBP detected in this work is shown in Supplementary material, Table S1.

$$CTI = \sum \left[\frac{C_x}{LC_{50x}} \right] \tag{1}$$

where CTI is the cytotoxicity index (mol/L), LC_{50} is the cytotoxicity value of each detected DBP (mol/L), and C_x is the production of each detected DBP (mol/L).

3. RESULTS AND DISCUSSION

3.1. DBPs formation with CN

The TCM, DCAN, and DCAA formed from CN are shown in Figure 2. It was noticed that the total DBPs concentration rapidly increased when CN was exposed to chlorine for more than 6 h (Figure 2(a)). The concentration of DCAN was much higher than the other two DBPs. The amounts of TCM, DCAN and DCAA were 4.94, 30.41, and 3.52 μg/L after 3 days of chlorination. Figure 2(b) shows that the concentration of DOC first increased and then remained stable. The residual chlorine continuously decreased and no free chlorine remained after 3 days. The time-dependent DON was shown in Supplementary material, Figure S1, which followed the same pattern as DOC. The concentration of DON reached 0.1 mg/L even in a short chlorination time (0.5 and 2 h), indicating that the reactivity between chlorine and CN was pretty high. The triazine ring of CN was composed of large amounts of nitrogen (Li *et al.* 2021a, 2021b). During the chlorination of CN, active chlorine might attack the nitrogen-containing groups of CN and promote the formation of chlorinated organics, which were the important components of DON and contained precursor sites of DCAN (Liu *et al.* 2018a, 2018b). Figure 2(c) compared the DBPs formation in the chlorination and chloramination processes. The DBPs amount decreased during the chloramination process, the concentration of TCM, DCAN and DCAA was 1.49, 3.96, and 1.11 μg/L after 3 days. These results were consistent with previous studies: chloramination might be a special case of chlorination with low Cl_2 generated from NH_2Cl hydrolysis and could effectively reduce the generation of DBPs (Zhou *et al.* 2014; Wei *et al.* 2017).

3.2. Factors affecting the formation of DBPs from CN

3.2.1. Effect of chlorine dosage

The chlorine dosage used in the disinfection process was an important factor that could significantly affect DBPs formation. As shown in Figure 3(a), the concentrations of TCM, DCAN, and DCAA were less than 5 μg/L at low chlorine dosage (1 and 4 mg/L as Cl_2) and the concentration of total DBPs increased with the improved chlorine dosage. The amount of DCAN was

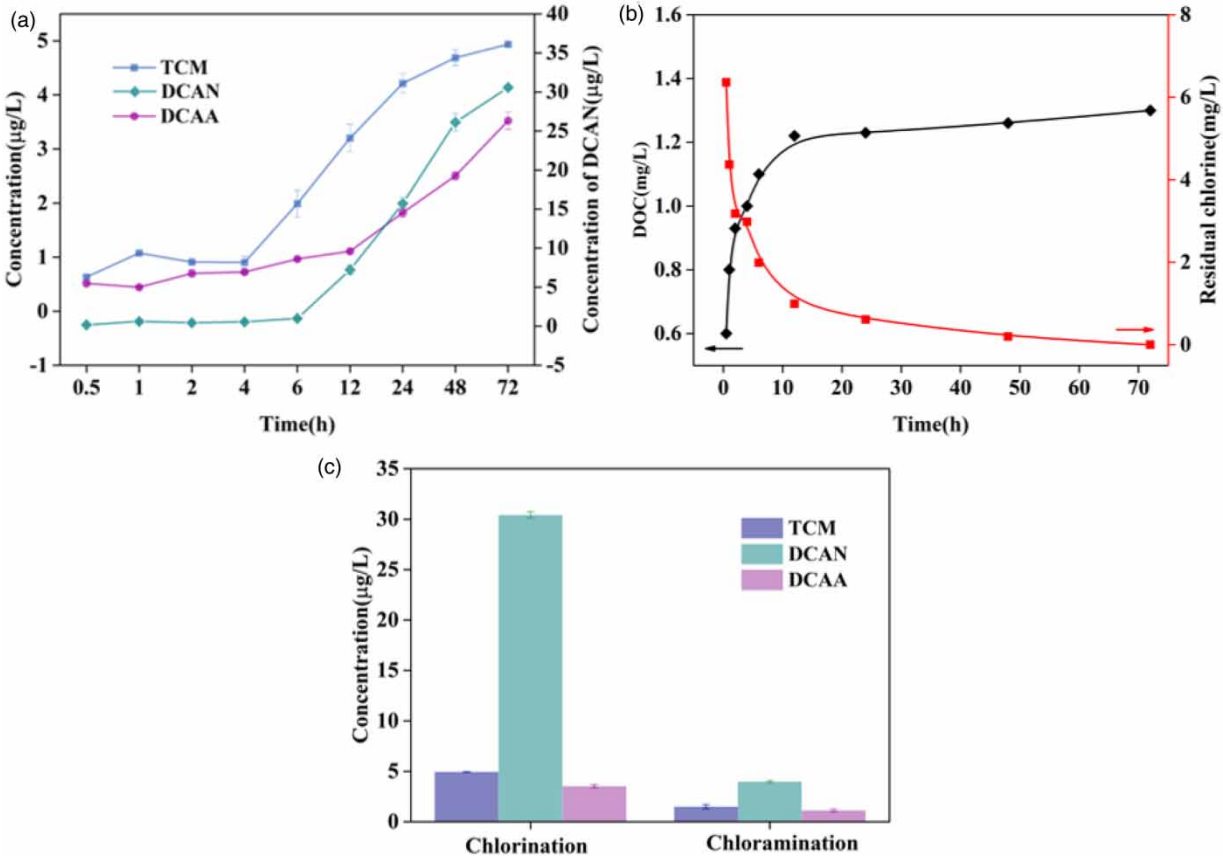

Figure 2 | (a) Time-dependent formation of TCM, DCAN and DCAA during chlorination of CN ([NaClO] = 20 mg/L as Cl_2, [CN] = 20 mg/L, pH = 7); (b) corresponding DOC concentration and residual chlorine during chlorination of CN; and (c) formation of TCM, DCAN and DCAA during chloramination ([NH_2Cl] = 20 mg/L as Cl_2, [CN] = 20 mg/L, pH = 7, reaction time = 3 days).

increased to 30.56 μg/L when the chlorine dosage was 20 mg/L. High concentrations of active chlorine promoted the drastic destruction of the triazine ring of CN to introduce organic nitrogen sources, thus promoting the formation of DCAN (Wang *et al.* 2012; Du *et al.* 2017).

3.2.2. Effect of pH

The effect of solution pH on TCM, DCAN, and DCAA formation with CN is depicted in Figure 3(b). The concentration of DCAN and DCAA increased as pH raised from 5 to 7, but decreased obviously when pH reached to 9, the total DBPs followed the same pattern. These results agreed with previous research (Ye *et al.* 2020), different pHs affected the morphology of HOCl, when pH < 7.5, HOCl was the major species. When pH reached 7.6, OCl− turned into the key species, which had less disinfectant potential, therefore less DCAN and DCAA were formed (Hu *et al.* 2015).

In addition, the excess hydroxide could assist the hydrolysis reactions of DCAN to produce stable THMs, which would lead to a higher concentration of TCM. Although OCl− had a high proportion under alkaline conditions, HOCl inevitably existed in the solution (Acero *et al.* 2005). The oxidative decomposition capacity of CN to produce nitrogen organics was greater than the alkaline catalytic hydrolysis ability of DCAN (Liu *et al.* 2018a, 2018b), thus DCAN was still the dominant species at pH = 9.

3.2.3. Effect of CN dosage

The results described above proved that CN was an important precursor of DBPs. Thus, the dosage of CN was a key factor affecting the formation of DBPs in the chlorination process. As shown in Figure 3(c), the increasing trend of total DBPs slowed down as CN dosage enhanced from 5 to 20 mg/L, which might be ascribed to the depletion of available chlorine. The effect of CN dosage on TCM and DCAA formation was not obvious, the amount of TCM and DCAA was 4.37 and

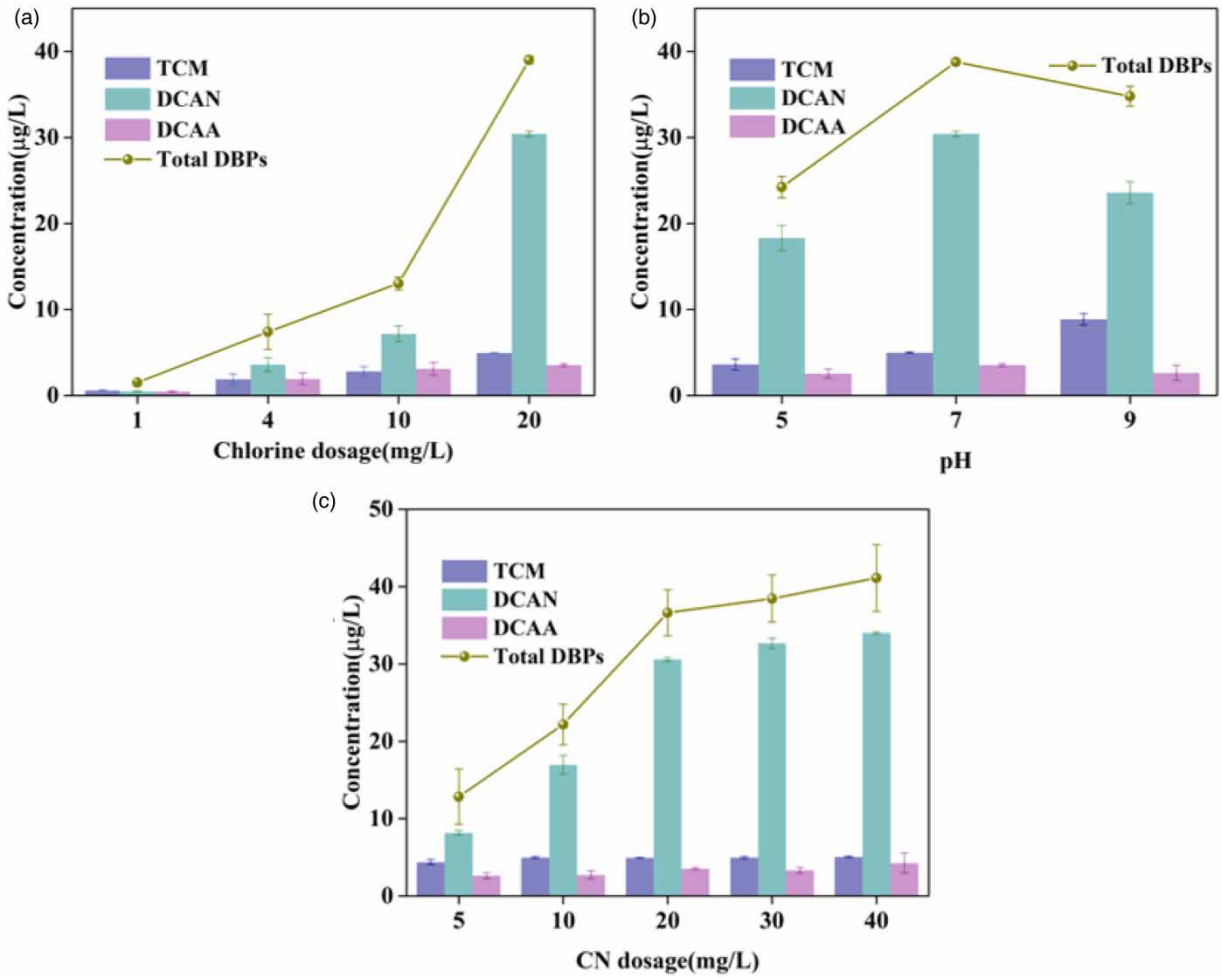

Figure 3 | (a) Effect of chlorine dosage on the formation of DBPs ([CN] = 20 mg/L, pH = 7, reaction time = 72 h). (b) Effect of pH on the formation of DBPs ([NaClO] = 20 mg/L as Cl_2, [CN] = 20 mg/L, reaction time = 72 h); and (c) effect of CN dosage on the formation of DBPs ([NaClO] = 20 mg/L as Cl_2, pH = 7, reaction time = 72 h).

2.61 μg /L at the lowest CN dosage, respectively. When CN dosage was increased to the maximum dosage, the concentration of TCM and DCAA was 5.05 and 4.25 μg/L. However, the concentration of DCAN enhanced nearly five times when CN dosage changed from 5 to 40 mg/L. The skeleton structure of CN was rich in nitrogen and with the increase of CN dosage, more nitrogen might be introduced to promote the formation of DCAN (Wang & Hu 2018; Cheng *et al.* 2020; Yan *et al.* 2022). These results indicated that CN had great potential for forming nitrogenous DBPs and fewer active precursor sites for the formation of carbonaceous DBPs.

3.3. Possible mechanism of CN-formed DBPs

The morphologies of CN before and after chlorination are shown in Figure 3. CN displayed a 2D lamellar-like morphology (Figure 4(a)) and it agglomerated after chlorination (Figure 4(b)). The AFM mages (Figures 4(c) and 4(d)) showed CN was fragmented and the thickness increased from 2.61 to 3.04 nm (Supplementary material, Figures S2 and S3) after chlorination, which was in good agreement with TEM results. CN and CN-Cl samples displayed Type IV isotherm (Supplementary material, Figure S4). Supplementary material, Table S2 shows the specific surface area of CN enhanced from 55.86 to 66.16 m^2/g as well as the average pore diameter increased from 10.93 to 13.82 nm after chlorination. These morphology changes of CN confirmed the reaction between chlorine and CN. The chlorine eroded the CN and caused damage to CN edges during the chlorination process.

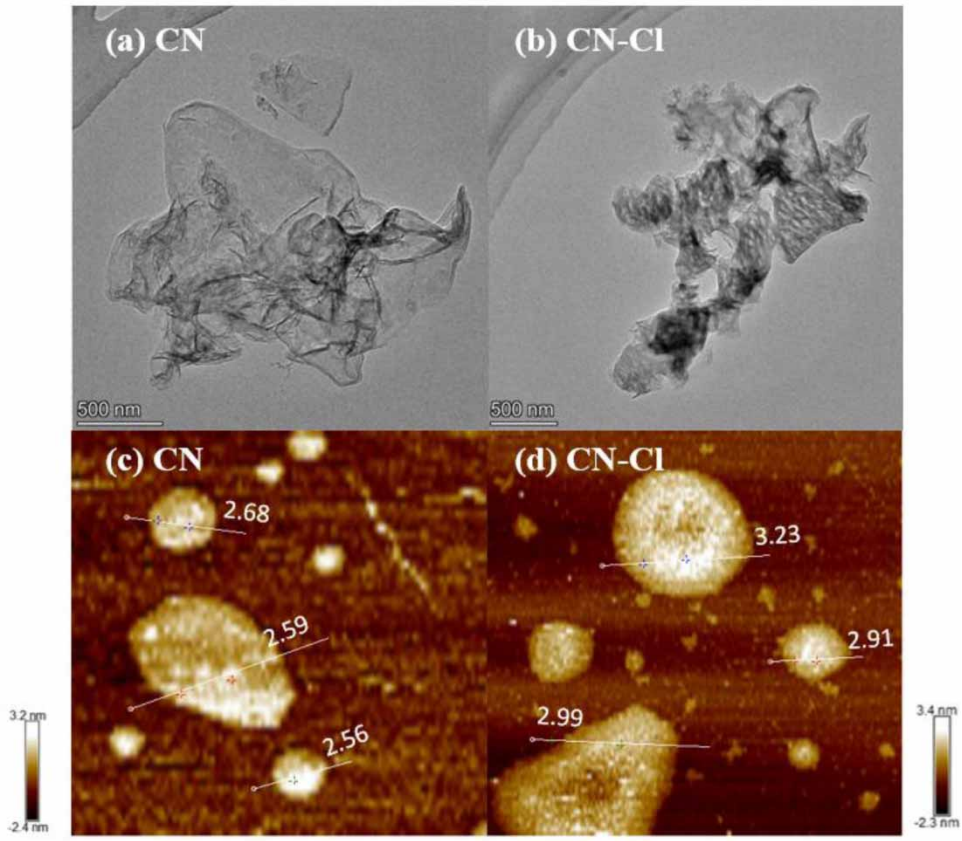

Figure 4 | TEM images of CN (a); CN-Cl (b); AFM images of CN (c); and CN-Cl (d).

Figure 5 reflects the surface chemical composition of CN after chlorination. The FTIR spectra was shown in Figure 5(a). Both CN and CN-Cl presented a sharp peak at 810 cm^{-1} and a broad peak at 1,200–1,700 cm^{-1}, which were attributed to the triazine units, C–N heterocycles, and aromatic C = N stretching vibration, respectively. Another broad peak at 3,000–3,600 cm^{-1} was the stretching vibrations of N–H and C–OH at the CN terminating edges (Liu *et al.* 2017a, 2017b; Wu *et al.* 2019). The characteristic peaks corresponding to triazine units and terminating groups weakened after the chlorination process. Figure 5(b) displayed the Raman spectra of CN and CN-Cl samples; Raman peaks at 709 (peak A) and 1,234 (peak B) cm^{-1} could be observed corresponding to the vibration modes of CN and heptazine heterocycles (Wang *et al.* 2016; Hafeez *et al.* 2018). The intensity of peaks A and B receded in CN-Cl sample, which further proved the destruction of N-containing aromatic rings of CN.

XPS was obtained to further investigate the CN surface chemical state variation after the chlorination process. As shown in Table 1, the surface oxygen and carbon properties were increased while the nitrogen content substantially decreased. In addition, similar to previous studies (Zhang *et al.* 2019; Huang *et al.* 2021), the surface chlorine content slightly increased after the chlorination process, which further proved the reaction between chlorine and carbon and nitrogen. Figure 5(c) showed the fully scanned spectra of CN and CN-Cl, the samples presented the three main peaks of O, N, and C. Due to the minimal chlorine content, no significant characteristic peaks were observed. Figures 5(d)–(f) showed the high-resolution C1s, N1s, and O1s spectra of CN and CN-Cl samples. The C1s peaks (Figure 5(d)) at 284.8, 285.6, 287.6, and 288.2 eV were attributed to C–C, N–C = N/C–O, C = O, and C–$(N)_3$. The peak corresponding to C–$(N)_3$ reduced, while the peak corresponding to C = O slightly improved in the CN-Cl sample. The N1s XPS spectra in Figure 5(e) were comprised of three peaks at 398.1, 398.8, and 400.4 eV, corresponding to CN = C, N–$(C)_3$ and the amino groups (N–H) at CN terminating edges. The peaks ascribed to N–$(C)_3$ and amino groups were significantly weakened in the CN-Cl sample. The O1s peaks (Figure 5(f)) at 531.6, 532.3, and 533.5 eV ascribed to C = O, surface H_2O, and C–O, respectively (Zhou *et al.* 2023; Xie *et al.* 2018; Chen *et al.* 2021). The C = O peak raised observably while the C–O peak decreased after chlorination, indicating oxidation

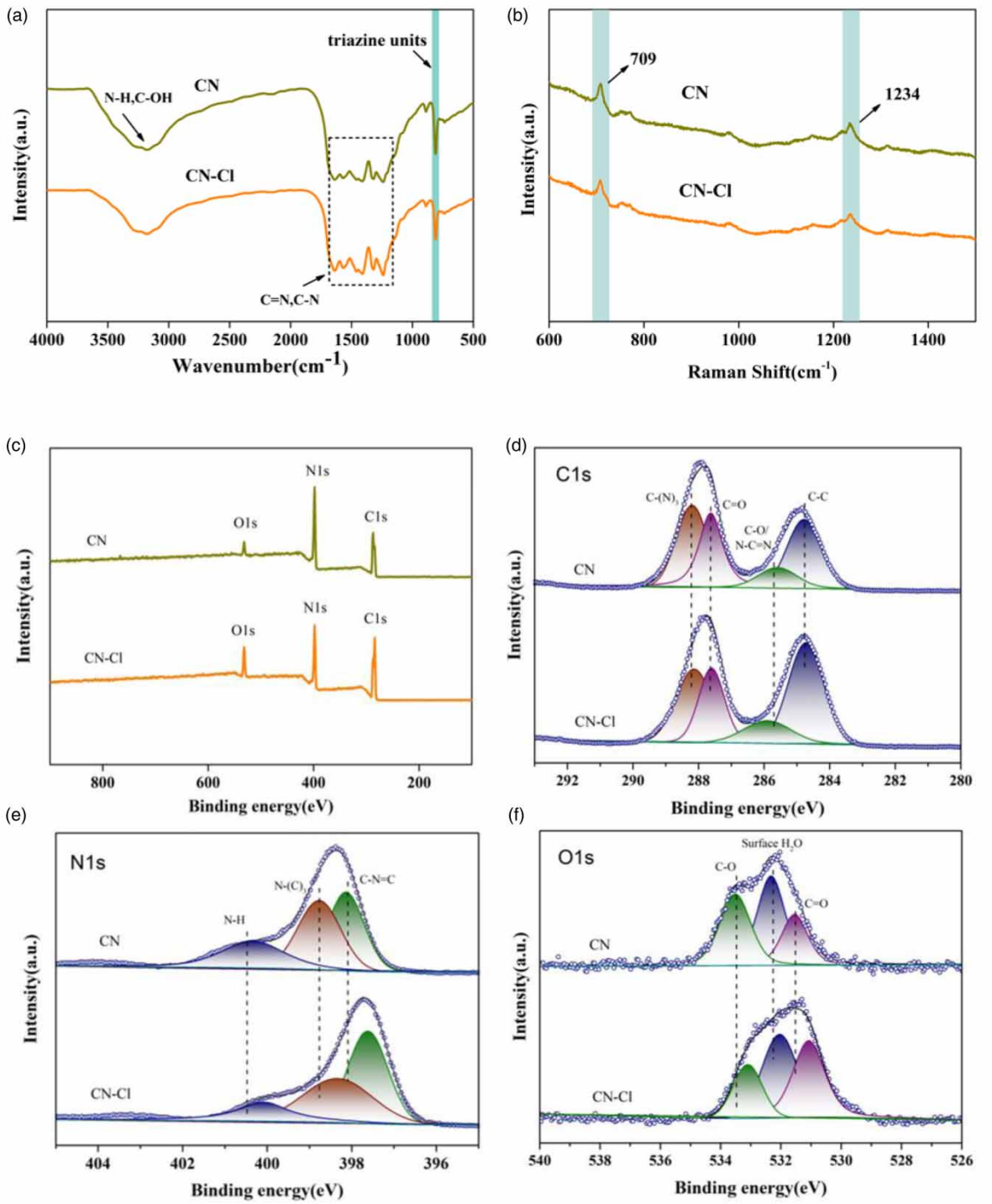

Figure 5 | FTIR spectrum of CN and CN-Cl (a); Raman Spectra of CN and CN-Cl (b); XPS spectra of survey (c); C1 s (d); N1s (e); and O1s (f) of initial CN and CN after chlorination (CN-Cl).

occurred on the surface of CN and formed additional O-containing functional groups, such as ketone, carboxyl, phenolic, alcohol, and ether.

These results suggested that chlorination of CN-produced DBPs might be via two mechanisms: (1) chlorine could destroy the triazine rings of CN by attacking C–$(N)_3$ and N–$(C)_3$ bonds, which promoted the formation of chlorinated organic

Table 1 | The surface C/N/O/Cl contents of samples

Sample	C (%)	N (%)	O (%)	Cl (%)
CN	51.42	44.46	4.12	–
CN-Cl	58.33	30.95	9.97	0.75

compounds and (2) chlorine might replace hydrogen of the amino groups on CN terminating edges to form chlorinated amino acids, which resulted in the most DCAN being formed.

3.4. DBPs formation and cytotoxicity of CN leaching solution

Since CN was synthesized from organic precursors, it was supposed that some small molecular organics might fall off the surface of CN and become potential DBPs precursors. Thus, the formation potential and theoretical cytotoxicity of DBPs of the CN leaching solution were investigated. Figure 6(a) shows the concentration of DBPs at different immersion times. DCAN was the dominant species and the concentration of DCAN was 5.65 μg/L at maximum leaching time, while the amount of TCM and DCAA was 3.08 and 1.75 μg/L, respectively. Figure 6(b) shows the concentration of DOC and residual chlorine of the leaching solution. The amount of DOC exhibited an increasing trend with the leaching time and remained at 0.5 mg/L after 3 days. The concentration of residual chlorine remained at 8.5 mg/L, which was significantly higher than that of direct chlorination. Supplementary material, Figure S5 shows that nitrogenous organics were dissolved in the leaching solution and the concentration of DON improved in the first 24 h and then remained at 0.15 mg/L. The theoretical cytotoxicity of the formed DBPs was estimated (Figure 6(c)). The CTI gradually improved with the extension of leaching time and the

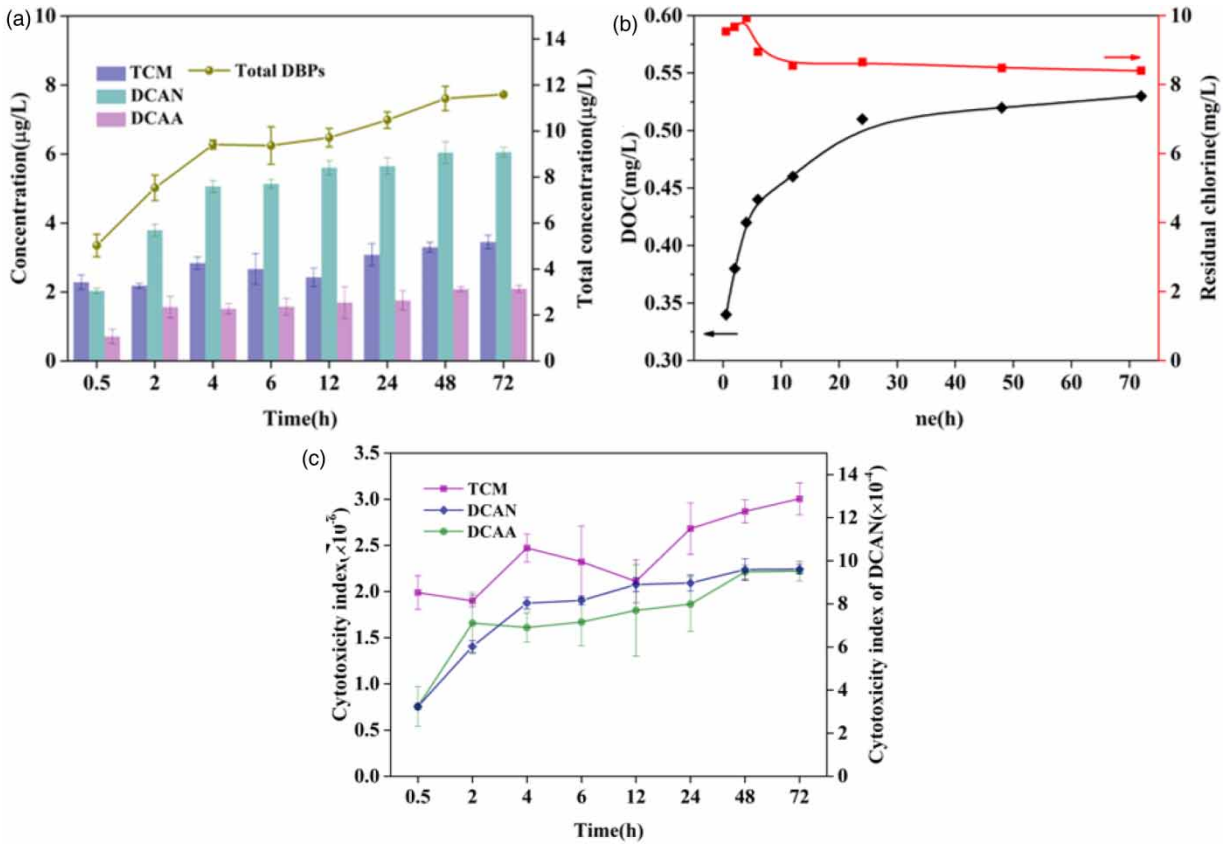

Figure 6 | Concentration of TCM, DCAN and DCAA in CN leaching solution with different leaching time (a); corresponding DOC and residual chlorine of the leaching solution (b); and corresponding theoretical cytotoxicity (c) ([NaClO] = 20 mg/L as Cl_2, [CN] = 20 mg/L, pH = 7, reaction time = 72 h).

toxicity of DCAN was two orders of magnitude higher than that of the other two DBPs. These results confirmed that CN could dissolve organics as important precursors of DCAN.

4. CONCLUSION

In this study, the DBPs formation potential of CN was analysed. TCM, DCAN, and DCAN could be produced by chlorination or chloramination of CN while chloramination could considerably lower the amount of DBPs. When chlorination time exceeded 6 h, the concentration of DBPs increased sharply and DCAN was the dominant species. Chlorine dosage, pH, and CN dosage could significantly affect the formation of the total DBPs and the effects on DCAN were the most significant. The destruction of C–$(N)_3$, N–$(C)_3$ bonds, and amino groups of CN by chlorine resulted in the formation of DBPs. Meanwhile, CN was able to leach organics in an aqueous solution, which was an important DBPs precursor. The released organics had a high activity with chlorine to form DBPs, particularly DCAN. The potential toxicity risks caused by leaching solutions were raised due to the increased immersion time of CN. These findings provided a reference for the potential environmental risks of CN; special attention should be paid when CN is exposed to chlorine. Reducing chlorine contacting time, controlling CN dosage, changing pH, reducing immersion time of CN, etc., were considered alternative options to reduce the formation potential of CN-formed DBPs.

ACKNOWLEDGEMENTS

This work was financially supported by the National Natural Science Foundation of China (Nos 51878357, 52170002, 51741807).

DECLARATION OF COMPETING INTEREST

The authors declare that they have no known competing financial interests or personal relationships that could have appeared to influence the work reported in this paper.

AUTHOR CONTRIBUTIONS

All authors contributed to the study's conception and design. L.N. conceptualized the system, investigated the study, wrote the original draft, reviewed and edited the file. J.H. developed the methodology, wrote the review, and edited the file. J.M. and H.W. supervised the study, wrote the review, and edited the file. S.L. developed the methodology, characterized the materials, wrote a review, and edited the file. J.L. conceptualized the system, supervised the study, managed project administration, acquired funds, wrote a review, and edited the file.

DATA AVAILABILITY STATEMENT

All relevant data are included in the paper or its Supplementary Information.

CONFLICT OF INTEREST

The authors declare there is no conflict.

REFERENCES

Acero, J. L., Piriou, P. & Gunten, U. V. 2005 Kinetics and mechanisms of formation of bromophenols during drinking water chlorination: assessment of taste and odor development. *Water Research* **39** (13), 2979–2993. https://doi.org/10.1016/j.watres.2005.04.055.

Acharya, R. & Parida, K. 2020 A review on TiO_2/g-C_3N_4 visible-light- responsive photocatalysts for sustainable energy generation and environmental remediation. *Journal of Environmental Chemical Engineering* **8** (4), 103896. https://doi.org/10.1016/j.jece.2020.103896.

Chen, J. X., Gao, N. Y., Li, L., Zhu, M. Q., Yang, J., Lu, X. & Zhang, Y. S. 2017 Disinfection by-product formation during chlor(am)ination of algal organic matters (AOM) extracted from microcystis aeruginosa: effect of growth phases, AOM and bromide concentration. *Environmental Science and Pollution Research* **24** (9), 1–10. https://doi.org/10.1007/s11356-017-8515-6.

Chen, J., Zhang, Y. G., Wu, B. F., Ning, Z. C., Song, M. Y., Zhang, H. F., Sun, X. Z., Wan, D. J. & Li, B. 2021 Porous g-C_3N_4 with defects for the efficient dye photodegradation under visible light. *Water Science and Technology* **84** (06), 1354–1365. https://doi.org/ 10.2166/wst.2021.313.

Cheng, Z., Ling, L., Wu, Z., Fang, J., Westerhoff, P. & Shang, C. 2020 Novel visible light-driven photocatalytic chlorine activation process for carbamazepine degradation in drinking water. *Environmental Science and Technology* **54**, 11584–11593. https://doi.org/10.1021/acs.est.0c03170.

Du, T. T., Adeleye, A. S., Keller, A. A., Wu, Z. N., Han, W., Wang, Y. Y., Zhang, C. D. & Li, Y. 2017 Photochlorination-induced transformation of graphene oxide: mechanism and environmental fate. *Water Research* **124**, 372–380. https://doi.org/10.1016/j.watres.2017.07.054.

Hafeez, H. Y., Lakhera, S. K., Bellamkonda, S., Rao, G. R., Shankar, M. V., Bahnemann, D. W. & Neppolian, B. 2018 Construction of ternary hybrid layered reduced graphene oxide supported g-C_3N_4-TiO_2 nanocomposite and its photocatalytic hydrogen production activity. *International Journal of Hydrogen Energy* **43** (8), 3892–3904. https://doi.org/10.1016/j.ijhydene.2017.09.048.

Han, J., Fu, R., Jin, C. Y., Li, Z. L., Wang, M., Yu, P. & Xie, Y. H. 2020 Highly sensitive detection of trace Hg^{2+} via PdNPs/g-C_3N_4 nanosheet-modified electrodes using DPV. *Microchemical Journal* **152**. https://doi.org/10.1016/j.microc.2019.104356.

Hu, C. Y., Cheng, M. & Lin, Y. L. 2015 Chlorination of bensulfuron-methyl: kinetics, reaction factors and disinfection by-product formation. *Journal of the Taiwan Institute of Chemical Engineers* **53**, 46–51. https://doi.org/10.1016/j.jtice.2015.02.029.

Huang, X., Yu, Y., Chen, H., Liang, H. K., Geng, M. Z. & Shi, B. Y. 2021 Disinfection by-product formation and toxicity evaluation for chlorination with powered activated carbon. *Water Research* **205**, 117660. https://doi.org/10.1016/j.watres.2021.117660.

Jazic, J. M., Agbaba, J., Tubic, A., Watson, M., Durkic, T., Krcmer, D. & Dalmacija, B. 2019 Effect of photochemical advanced oxidation processes on the formation potential of emerging disinfection by-products in groundwater from part of the Pannonian Basin. *Water Supply* **19** (5-6), 1388–1395. https://doi.org/10.2166/ws.2018.196.

Jeong, C. H., Postigo, C., Richardson, S. D., Simmons, J. E., Kimura, S. Y., Marinas, B. J., Barcelo, D., Liang, P., Wagner, E. D. & Plewa, M. J. 2015 Occurrence and comparative toxicity of haloacetaldehyde disinfection byproducts in drinking water. *Environmental Science & Technology* **49** (23), 13749. https://doi.org/10.1021/es506358x.

Jiang, Y. J., Guan, D., Liu, Y. M., Yin, X. Q., Zhou, S., Zhang, G. L., Wang, N. & Sun, H. M. 2020 The transport of graphitic carbon nitride in saturated porous media: effect of hydrodynamic and solution chemistry. *Chemosphere* **248**, 125973. https://doi.org/10.1016/j.chemosphere.2020.125973.

John, A., Rajan, M. S. & Thomas, J. 2021 Carbon nitride-based photocatalysts for the mitigation of water pollution engendered by pharmaceutical compounds. *Environmental Science and Pollution Research* **28**, 24992–25013. https://doi.org/10.1007/s11356-021-13528-y.

Li, M., Sun, J., Wang, D. D., Zhang, R., Wang, H. B. & Wang, N. 2021a Using potassium ferrate control hazardous disinfection by-products during chlorination. *Environmental Science and Pollution Research* **28**, 54137–54146. https://doi.org/10.1007/s11356-021-14525-x.

Li, X., Huang, G. H., Chen, X. J., Huang, J., Li, M. N., Yin, J. A., Liang, Y., Yao, Y. & Li, Y. P. 2021b A review on graphitic carbon nitride (g-C_3N_4) based hybrid membranes for water and wastewater treatment. *Science of The Total Environment* **792**, 148462. https://doi.org/10.1016/j.scitotenv.2021.148462.

Liu, C. Y., Zhang, Y. H., Dong, F., Reshak, A. H., Ye, L. Q., Pinna, N., Zeng, C., Zhang, T. R. & Huang, H. W. 2017a Chlorine intercalation in graphitic carbon nitride for efficient photocatalysis. *Applied Catalysis B: Environmental* **203**, 465–474. https://doi.org/10.1016/j.apcatb.2016.10.002.

Liu, S. Z., Ke, J., Sun, H. Q., Liu, P., Tade, M. O. & Wang, S. B. 2017b Size dependence of uniformed carbon spheres in promoting graphitic carbon nitride toward enhanced photocatalysis. *Applied Catalysis B: Environmental* **204**, 358–364. https://doi.org/10.1016/j.apcatb.2016.11.048.

Liu, C., Ersan, M. S., Plewa, M. J., Amy, G. & Karanfil, T. 2018a Formation of regulated and unregulated disinfection byproducts during chlorination of algal organic matter extracted from freshwater and marine algae. *Water Research* **142**, 313–324. https://doi.org/10.1016/j.watres.2018.05.051.

Liu, M. M., Zhang, M., Hao, R. J., Du, T. T., Li, T. & Li, Y. 2018b Disinfection byproduct formation and toxicity of graphene oxide in water treatment system. *Chemosphere* **207** (2019), 68–75. https://doi.org/10.1016/j.chemosphere.2018.10.165.

Ren, Z., Chen, S., Jiang, S. F., Hu, W. F. & Jiang, H. 2021 High-efficiency and ground-state atomic oxygen-dominant photodegradation of carbamazepine by coupling chlorine and g-C_3N_4. *Industrial & Engineering Chemistry Research* **60** (5). https://doi.org/10.1021/acs.iecr.0c05522.

Santosoa, E., Ediatia, R., Kusumawatia, Y., Bahruji, H., Sulistiono, D. O. & Prasetyoko, D. 2020 Review on recent advances of carbon based adsorbent for methylene blue removal from waste water. *Materials Today Chemistry* **16**, 100233. https://doi.org/10.1016/j.mtchem.2019.100233.

Stefán, D., Erdélyi, N., Izsák, B., Zaray, G. & Vargha, M. 2019 Formation of chlorination by-products in drinking water treatment plants using breakpoint chlorination. *Microchemical Journal* **149**, 104008. https://doi.org/10.1016/j.microc.2019.104008.

Wagner, E. D. & Plewa, M. J. 2017 CHO cell cytotoxicity and genotoxicity analyses of disinfection by-products: an updated review. *Journal of Environmental Sciences* **58** (8), 64–76. https://doi.org/10.1016/j.jes.2017.04.021.

Wang, L. & Hu, J. 2018 Formation of disinfection by-products in remineralized desalinated seawater with bacterial materials as precursor. *Desalination* **441**, 1–8. https://doi.org/10.1016/j.desal.2018.04.022.

Wang, C., Shang, C., Ni, M. L. & Jiang, F. 2012 (Photo)chlorination-induced physicochemical transformation of aqueous fullerene nc60. *Environmental Science & Technology* **46** (17), 9398–9405. https://doi.org/10.1021/es301037f.

Wang, P., Sun, S. H., Zhang, X. Y., Ge, X. & Lu, W. 2016 Efficient degradation of organic pollutants and hydrogen evolution by g-C_3N_4 using melamine as the precursor and urea as the modifier. *RSC Advances* **6** (40), 33589–33598. https://doi.org/10.1039/c5ra26890g.

Wang, A. W., Wang, C. D., Fu, L., Wong-Ng, W. & Lan, Y. C. 2017 Recent advances of graphitic carbon nitride-based structures and applications in catalyst, sensing, imaging, and LEDs. *Nano-Micro Letters* **9** (4). https://doi.org/10.1007/s40820-017-0148-2.

Wei, X., Gao, N. & Li, C. 2017 Evaluation and reduction of THMs, DCAN and TCNM formation potential from chlorination and chloramination of verapamil. *Journal of Environmental Chemical Engineering* **5** (5), 4397–4405. https://doi.org/10.1016/j.jece.2017.08.025.

Wongrueng, A., Rakruam, P., Siri, A. & Siyasukh, A. 2019 Synthesis of porous pig bone char as adsorbent for removal of DBP precursors from surface water. *Water Science and Technology* **79** (05), 857–865. https://doi.org/10.2166/wst.2018.486.

Wu, X. H., Wang, X. F., Wang, F. Z. & Yu, H. G. 2019 Soluble g-C_3N_4 nanosheets: facile synthesis and application in photocatalytic hydrogen evolution. *Applied Catalysis B Environmental* **247**, 70–77. https://doi.org/10.1016/j.apcatb.2019.01.088.

Xie, Z. J., Feng, Y. P., Wang, F. L., Chen, D. N., Zhang, Q. X., Zeng, Y. Q., Lv, W. Y. & Liu, G. G. 2018 Construction of carbon dots modified MoO_3/g-C_3N_4 Z-scheme photocatalyst with enhanced visible-light photocatalytic activity for the degradation of tetracycline. *Applied Catalysis B: Environmental* **229**, 96–104. https://doi.org/10.1016/j.apcatb.2018.02.011.

Yan, X. S., Lin, T., Wang, X. X., Zhang, S. S. & Zhou, K. M. 2022 Effects of pipe materials on the characteristic recognition, disinfection byproduct formation, and toxicity risk of pipe wall biofilms during chlorination in water supply pipelines. *Water Research* **210**, 117980. https://doi.org/10.1016/j.watres.2021.117980.

Yang, Y., Li, X., Zhou, C. Y., Xiong, W. P., Zeng, G. M., Huang, D. L., Zhang, C., Wang, W. J., Song, B. A., Tang, X., Li, X. P. & Guo, H. 2020 Recent advances in application of graphitic carbon nitride-based catalysts for degrading organic contaminants in water through advanced oxidation processes beyond photocatalysis: a critical review. *Water Research* **184**, 116200. https://doi.org/10.1016/j.watres.2020.116200.

Ye, Z. X., Shao, K. L., Huang, H. & Yang, X. 2020 Tetracycline antibiotics as precursors of dichloroacetamide and other disinfection byproducts during chlorination and chloramination. *Chemosphere* **270**, 128628. https://doi.org/10.1016/j.chemosphere.2020.128628.

Zhang, M., Wang, X., Du, T. T., Wang, H. H., Hao, H. Z., Wang, Y. Y., Li, Y. & Hao, T. W. 2019 Effects of carbon materials on the formation of disinfection byproducts during chlorination: pore structure and functional groups. *Water Research* **16**, 1–10. https://doi.org/10.1016/j.watres.2019.06.059.

Zhou, S. Q., Shao, Y. S., Gao, N. Y., Zhu, S. M., Ma, Y. & Deng, J. 2014 Chlorination and chloramination of tetracycline antibiotics: disinfection by-products formation and influential factors. *Ecotoxicology and Environmental Safety* **107**, 30–35. https://doi.org/10.1016/j.ecoenv.2014.05.008.

Zhou, Q. X., Song, C. L., Wang, P. F., Zhao, Z. Y., Li, Y. & Zhan, S. H. 2023 Generating dual active species by triple-atom-sites through peroxymonosulfate activation for treating micropollutants in complex water. *Proceedings of the National Academy of Sciences of the United States of America* **102** (13). https://doi.org/10.1073/pnas.2300085120.

Zhu, B. C., Zhang, L. Y., Cheng, B. & Yu, J. G. 2018 First-principle calculation study of tri-s-triazine-based g-C_3N_4: a review. *Applied Catalysis B: Environmental* **224**, 983–999. https://doi.org/10.1016/j.apcatb.2017.11.025.

First received 28 October 2022; accepted in revised form 12 March 2023. Available online 23 March 2023